Phase-Plane-Derived Distortion Modeling of a Fast and Accurate Digitizing Sampler

David I. Bergman, *Member, IEEE*, and Gerard N. Stenbakken, *Member, IEEE*

***Abstract*—Continued efforts to model the distortion behavior of custom-designed digitizing samplers for accurate measurement of dynamic signals are reported. This work is part of ongoing efforts at the National Institute of Standards and Technology (NIST) to advance the state of the art in waveform sampling metrology. In this paper, an analytic error model for a sampler having a −3-dB 6-GHz bandwidth is described. The model is derived from examination of the sampler's error behavior in the phase plane. The model takes as inputs the per-sample estimates of signal amplitude, first derivative, and second derivative, where the derivatives are with respect to time. The model's analytic form consists of polynomials in these terms, which are chosen from consideration of the voltage dependence of the digitizer input capacitance and the previously studied error behavior in a predecessor digitizer. At 1 GHz, an improvement in total harmonic distortion from −32 to −46 dB is obtained when model-generated sample corrections are applied to the waveform. The effect of timebase distortion in the sampling system is also accounted for and corrected. The inclusion of second-derivative dependence in the model is shown to improve the model's fit to the measured data by providing fine temporal adjustment of the fitted waveform.**

***Index Terms*—Analog-to-digital conversion, data models, error compensation, nonlinear distortion, signal sampling.**

I. Introduction

CONTINUED advances in the development of high-speed signal generators and samplers require control and minimization of errors arising from dynamic nonlinear behavior commonly referred to as distortion. In some applications, the intrinsic distortion performance of signal generating and sampling equipment can be improved through numeric preprocessing of digital data patterns for waveform synthesis or postprocessing of acquired data samples. One example is the modeling of distortion behavior for base station power amplifiers to produce compensating predistorted data patterns for greater power efficiency and reduced adjacent channel leakage [1]. Another example is the calibration of multisine signals used to characterize radio frequency (RF) devices for wireless applications [2].

This paper describes a data processing method to correct nonlinear dynamic error in a sampling probe having a −3-dB 6-GHz bandwidth. We report a 14-dB improvement in achievable total harmonic distortion (THD), which is from −32 to −46 dB at 1 GHz for a signal with a peak amplitude of 1.6 V. This work is part of the continuing efforts of the National Institute of Standards and Technology (NIST) to establish, maintain, and provide accurate waveform sampling metrology for signals having a frequency content from dc to 1 GHz. The sampler under study is similar to two NIST-developed sampling probes previously described [3], [4]. All of these probes are noteworthy for their excellent gain flatness and settling performance. However, because they exhibit more harmonic distortion than is typically seen in track-and-hold-type samplers with comparable bandwidth, an investigation into the efficacy of postsampling data processing to improve THD was undertaken.

We have previously described an error model [5] that is able to reduce dynamic errors in a NIST-designed low-bandwidth sampling probe [3] over the frequency range of dc–1 MHz. Although that digitizer and the one of interest here are constructed with different technologies and have considerable performance differences in terms of speed and accuracy, they share a common principle of operation and many architectural similarities. It is therefore believed that a modeling approach similar to the one developed for the slow digitizer will be effective at describing the error behavior of the fast probe. Results so far suggest that this assumption is reasonable.

II. Background

The digitizer we are modeling has a sampling-comparator architecture. We refer to it as the next-generation sampling-comparator (NGSC) probe because it is the follow-up to an earlier NIST-designed probe [4]. The NGSC probe utilizes a semicustom layout in bipolar Si technology ($f_T = 26$ GHz). Like its predecessor and the low-bandwidth probe, the NGSC probe was designed specifically to offer high performance in gain flatness and settling error, which are parameters of interest to NIST measurement services [6]. A simplified circuit schematic of the comparator section of the NGSC probe is shown in Fig. 1.

Phase-plane compensation for analog-to-digital converters (ADCs) has been discussed extensively in the literature [7]–[13]. In past efforts to characterize the distortion behavior of NIST-designed sampling probes, a distortion model was derived experimentally from examination of the probe's error surface in the phase plane spanned by signal state and slope [5]. We found that a linear combination of basis functions consisting of seventh-order polynomials in state, first derivative, and second derivative did a good job of describing the digitizer's dynamic error behavior. Of significant consequence was the finding that the prescribed manner in which the second-derivative terms were introduced endowed the model with the

Manuscript received June 15, 2005; revised April 17, 2006. This work was supported by the Electronics and Electrical Engineering Laboratory, Technology Administration, U.S. Department of Commerce.

The authors are with the National Institute of Standards and Technology (NIST), Gaithersburg, MD 20899 USA (e-mail: dbergman@nist.gov).

Digital Object Identifier 10.1109/TIM.2006.876534

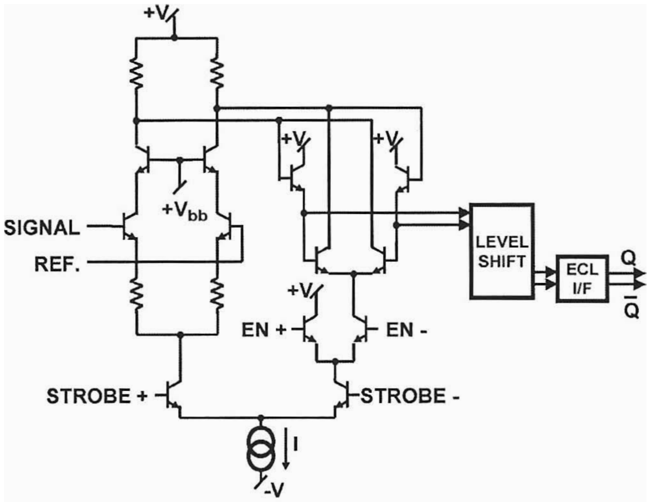

Fig. 1. Simplified schematic of comparator, highlighting critical circuitry.

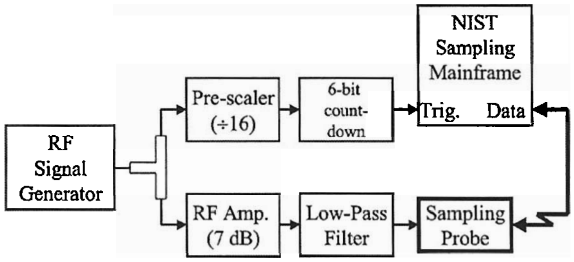

Fig. 2. Measurement setup.

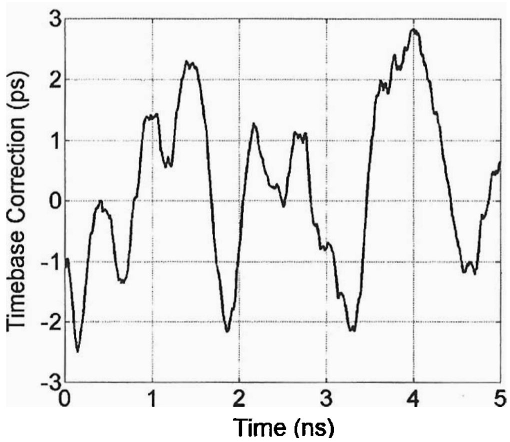

Fig. 3. Timebase corrections.

correct relationship between harmonic distortion and nonlinear gain and phase error, which are not easily measured. The method provided a complete description of the error behavior of the probe, including nonlinear gain, phase, and offset error in addition to harmonic distortion from measurements of probe harmonic distortion alone.

In this paper, we deviate from the earlier modeling approach in two regards: First, timebase nonlinearity was not a concern previously because the signal frequencies were relatively low. For this paper, signal frequencies are high enough that timebase nonlinearity can introduce errors that are not benign to the modeling process. We address this issue by using curve fitting to sinusoidal reference signals [14] to separate the errors inherent to the sampler from those resulting from timebase nonlinearity. Second, we found previously that an input capacitance model based on the customary expression for p-n junction capacitance [15] was effective at improving the model's fit to probe-distortion behavior. In this paper, we instead model input capacitance error with a Taylor series approximation, which has been found to consist of a polynomial in state–slope cross-product terms [11]. We note in passing that, as shown in Fig. 1, the NGSC probe uses a cascode input-stage configuration that reduces Miller multiplication of the input capacitance and the attendant contribution of its voltage nonlinearity to probe distortion.

III. Data Collection

In order to examine the error behavior of the probe in the phase plane, we measured an ensemble of calibration sine waves over a peak amplitude range of 0.1–1.6 V using the measurement setup shown in Fig. 2. The probe's full-scale range is ±1.8 V. The signal source was a commercial RF signal generator. Timing jitter between the generator's signal output and its synchronous timebase output made the timebase signal unsuitable as a trigger for the sampling mainframe. The mainframe's trigger signal was therefore derived from the test signal through a prescaler and countdown chain. The measurement epoch duration was 5 ns. We collected two amplitude ensembles: one at a frequency of 1 GHz and one at a frequency of 600 MHz. Thus, for the 1-GHz data, there were exactly five waveform periods contained in the data records, whereas for the 600-MHz data, there were exactly three waveform periods contained in the data records. An analog low-pass filter was used to ensure adequate spectral purity of the test signals. The attenuation of the filter was approximately −30 and −80 dB at 1.2 and 2 GHz, respectively. The specified harmonic and spurious signal levels of the signal generator and RF amplifier were better than −30 dBc. The RF amplifier had a low-frequency corner at 20 MHz. Therefore, any changes in the dc offset of the measured data could be attributed only to distortion behavior in the sampler and not to the signal source.

To account for nonlinearity in the timebase that would affect estimates of the probe's harmonic distortion, a timebase correction vector was computed using calibration signals at 1 GHz and 900 MHz, with each at four phases (0°, 90°, 180°, and 270°) [14]. The resulting timebase correction vector is shown in Fig. 3, and the effect of these corrections is shown in Fig. 4 where the residual error of a three-parameter sine fit [16], [17] to measured probe data is shown. When timebase nonlinearity is corrected, the structure in the fit residuals per waveform period repeats with better uniformity. The corrections in Fig. 3 have been smoothed with a nine-point moving average filter. Timebase corrections were used in all subsequent data processing.

IV. Error Modeling

In consideration of previous work [18] suggesting that probe dynamic error depended only on powers (quadratic and higher)

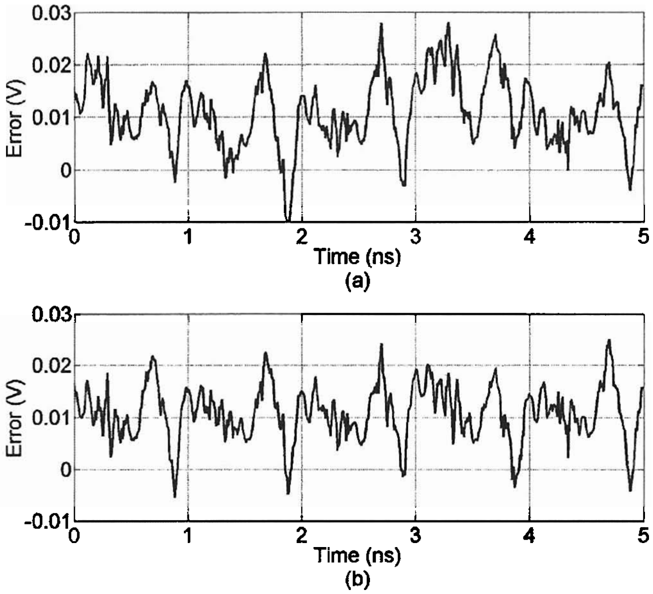

Fig. 4. Probe distortion for a 0.7-V 1-GHz signal (a) without timebase correction and (b) with timebase correction.

of first-derivative signal (slope), we previously [5] used as many powers of slope as were advised by the number of significant harmonic components in the error spectrum. For this paper, we continue this approach for the simple reason that it appears to be effective. We also make use of the finding [11] that the error caused by interaction of a nonzero resistive source impedance with probe voltage-dependent input capacitance can be modeled with the form $p(\boldsymbol{y})\dot{\boldsymbol{y}}$, where the notation $\boldsymbol{y}$ indicates the vector of sampled data and $\dot{\boldsymbol{y}}$ indicates the first derivative of the vector $\boldsymbol{y}$ with respect to time. The polynomial $p(\boldsymbol{y})$ is a simple power series in $\boldsymbol{y}$. We have determined from studying different error models that a model combining these two sets of basis functions can describe most of the error behavior shown in Fig. 4. In addition, we have found that the inclusion of the first derivative with respect to time of each of these error terms improves the fit to the data by producing a fine adjustment to the temporal positioning of the modeled error.

An explanation of the procedure begins by writing the error behavior modeled by the powers of slope as

$$e = \sum_{i=1}^{n} w_i \dot{y}^{i+1} = A_0 w \tag{1}$$

where $\boldsymbol{A}_0$ is an $m \times n$ matrix whose columns are model basis functions and whose rows correspond to data samples, $\boldsymbol{w}$ is an $n \times 1$ vector of regression coefficients, and $\boldsymbol{e}$ is an $m \times 1$ vector of probe errors obtained from sine fit residuals or the discrete Fourier transform (DFT). From (1), $\boldsymbol{A}_0 = [\dot{\boldsymbol{y}}^2, \dot{\boldsymbol{y}}^3, \ldots, \dot{\boldsymbol{y}}^{n+1}]$. Because we are using timing corrections and therefore do not have uniform sample spacing, we compute $\boldsymbol{e}$ using sine wave curve fitting. As the residual of a sine fit, the vector $\boldsymbol{e}$ contains no fundamental.

The full model matrix $\boldsymbol{A}$, which contains all the error components described previously, is comprised of four $m \times n$ submatrices such that

$$A = [A_0, A_1, A_2, A_3] \tag{2}$$

where

$$A_1 = [y\dot{y}, y^2\dot{y}, \ldots, y^n\dot{y}] \tag{2a}$$

$$A_2 = [\dot{y}\ddot{y}, \dot{y}^2\ddot{y}, \ldots, \dot{y}^n\ddot{y}] \text{ and} \tag{2b}$$

$$A_3 = [y\ddot{y} + \dot{y}^2, y^2\ddot{y} + 2y\dot{y}^2, \ldots, y^n\ddot{y} + ny^{n-1}\dot{y}^2]. \tag{2c}$$

The notation $\ddot{\boldsymbol{y}}$ indicates the second derivative of the vector $\boldsymbol{y}$ with respect to time. The $\boldsymbol{A}_1$ model components describe nonlinear input capacitance error. The columns of $\boldsymbol{A}_2$ and $\boldsymbol{A}_3$ are the time derivatives of the functions comprising the columns of $\boldsymbol{A}_0$ and $\boldsymbol{A}_1$, respectively.

Fitting the harmonic content of the model to the harmonic content of the probe requires solving the system of linear equations

$$e = \tilde{A} w \tag{3}$$

where $\tilde{\boldsymbol{A}}$ equals $\boldsymbol{A}$ with the fundamental component removed from each column.

As has been noted previously [11], a better determination of $\boldsymbol{w}$ is obtained with a global fit to multiple calibration signals of different amplitudes and frequencies. With multiple calibration signals, (3) becomes

$$\begin{bmatrix} e^{(1)} \\ e^{(2)} \\ \vdots \\ e^{(L)} \end{bmatrix} = \begin{bmatrix} \tilde{A}^{(1)} \\ \tilde{A}^{(2)} \\ \vdots \\ \tilde{A}^{(L)} \end{bmatrix} w$$

$$e_{\mathrm{L}} = \tilde{A}_{\mathrm{L}} w = \tilde{A}_{\mathrm{L}} K w^* \tag{4}$$

where L is the number of calibration signals. The diagonal matrix $\boldsymbol{K}(4n \times 4n)$ is introduced to provide the normalized design matrix $\tilde{\boldsymbol{A}}_{\mathrm{L}}\boldsymbol{K}$. The elements of $\boldsymbol{K}$ are the reciprocal of the root mean square (rms) of each of the columns of $\tilde{\boldsymbol{A}}_{\mathrm{L}}$. From (4), $\boldsymbol{w}^*$ can be estimated in a least squares sense as

$$w^* \approx \hat{w}^* = \left[(\tilde{A}_{\mathrm{L}}K)^{\mathrm{T}}(\tilde{A}_{\mathrm{L}}K)\right]^{-1} (\tilde{A}_{\mathrm{L}}K)^T e_{\mathrm{L}}. \tag{5}$$

With $\hat{\boldsymbol{w}}^*$ determined, errors in a given set of sampled data are modeled by computing

$$\hat{e} = A_{\mathrm{x}} K \hat{w}^* \tag{6}$$

where each column of $\boldsymbol{A}_{\mathrm{x}}$ is computed from the analytic expression for the corresponding column in $\boldsymbol{A}$ but reevaluated using the state and derivative values from the sampled data being corrected. We note that because the functions in $\boldsymbol{A}_{\mathrm{x}}$ contain fundamental, $\hat{e}$ includes an estimate of error at the fundamental frequency.

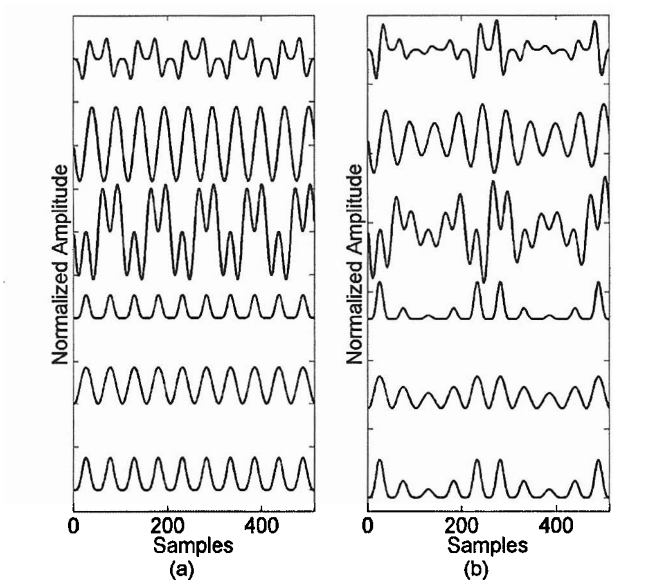

Fig. 5. Six most significant model functions ($n = 5$) generated from (a) pure sine wave and (b) modulated sine wave input.

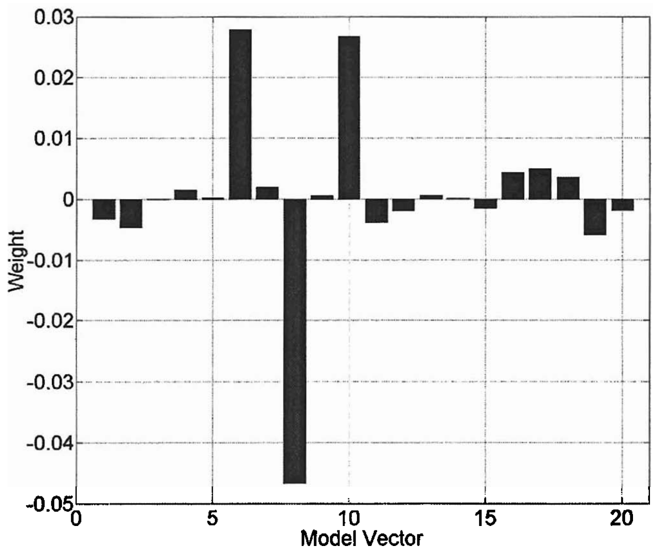

Fig. 6. Model coefficients $\hat{w}^*$.

A key attribute of this method is that a single set of regression coefficients $\hat{w}^*$ can correct errors in any arbitrary signal because the basis functions that make up the error estimate are recomputed for each new waveform being corrected. As an example, Fig. 5 illustrates the patterns of the six most significantly weighted columns of $\boldsymbol{A}_x\boldsymbol{K}$ generated by an 800-MHz sine wave with a peak amplitude of 1.5 V and by the same signal with 20% amplitude modulation at 320 MHz.

Fig. 6 plots the regression coefficients resulting from fitting the model to the 600-MHz and 1-GHz calibration signals. Most of the probe's error behavior is described by the $\boldsymbol{A}_1$ components of the model (specifically, the $y\dot{y}$, $y^3\dot{y}$, and $y^5\dot{y}$ terms), although some of the $\boldsymbol{A}_0$, $\boldsymbol{A}_2$, and $\boldsymbol{A}_3$ components are significant as well.

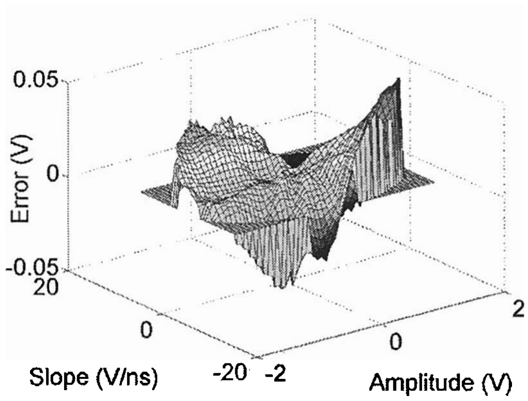

Fig. 7. Error surface for 1-GHz data.

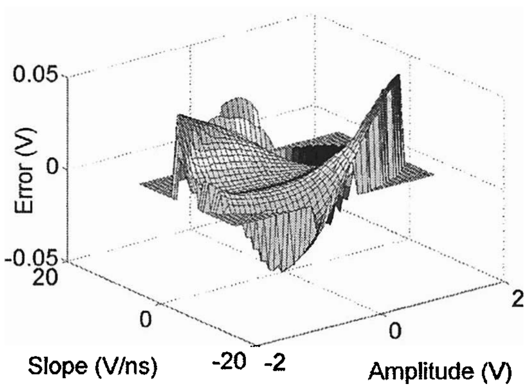

Fig. 8. Model-generated corrections for 1-GHz data.

V. Results

The NGSC probe's error surface in state–slope space after binning the time-domain errors from the test signal ensemble is shown in Fig. 7. The surface was generated from 1-GHz data. Model-generated corrections using a model order $n = 5$ are shown in Fig. 8. For comparison with Fig. 7, the fundamental component in the corrections has been removed. Figs. 7 and 8 show good agreement between the data and the modeled fit to the data.

Figs. 9 and 10 show the model's performance in the frequency domain as a function of input signal level. The model was fit to the 600-MHz and 1-GHz calibration ensemble excluding those signals whose peak amplitudes were less than 1 V. This choice produced the best agreement between the model and the data for large signals, where distortion is of greatest concern. In Fig. 9, the magnitudes of the second, third, and fourth harmonics of measured and modeled data are plotted. Here, we see excellent agreement between measured and modeled harmonics at 1 GHz. At 600 MHz, the modeled third harmonic fits well at higher signal levels, whereas the modeled second harmonic fits the data best for signal levels between approximately 0.8 and 1.3 V.

In Fig. 10, the phase difference between measured and modeled data for the second, third, and fourth harmonics is plotted versus the input signal level. At 1 GHz, the model produces excellent phase agreement for the second harmonic and good

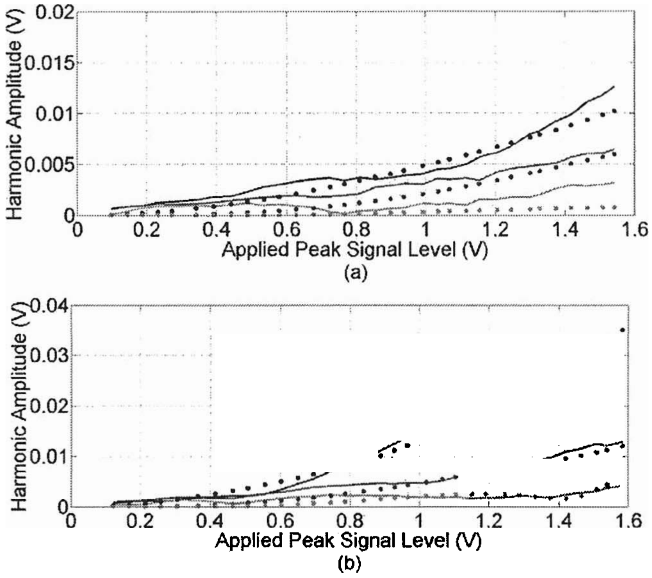

Fig. 9. Measured (solid line) and modeled (dotted line) magnitude of second (darkest), third, and fourth (lightest) harmonics versus input signal level for (a) 600-MHz and (b) 1-GHz measurement ensembles.

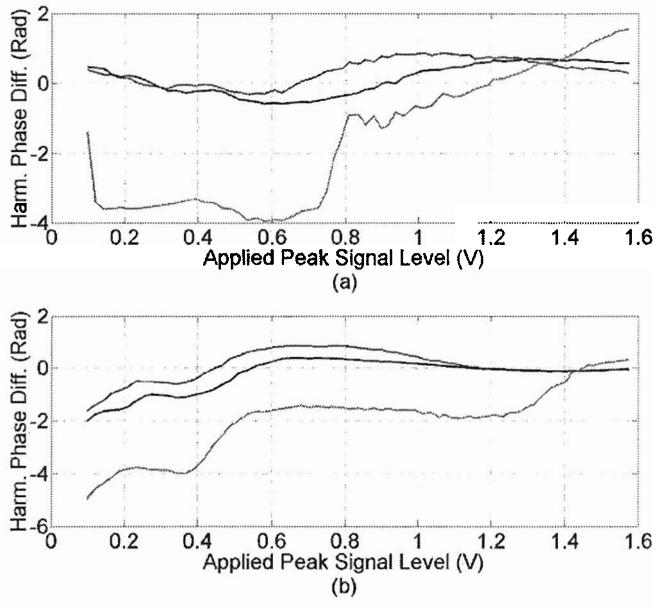

Fig. 10. Phase difference between measured and modeled data for second (darkest), third, and fourth (lightest) harmonics versus input signal level for (a) 600-MHz and (b) 1-GHz measurement ensembles.

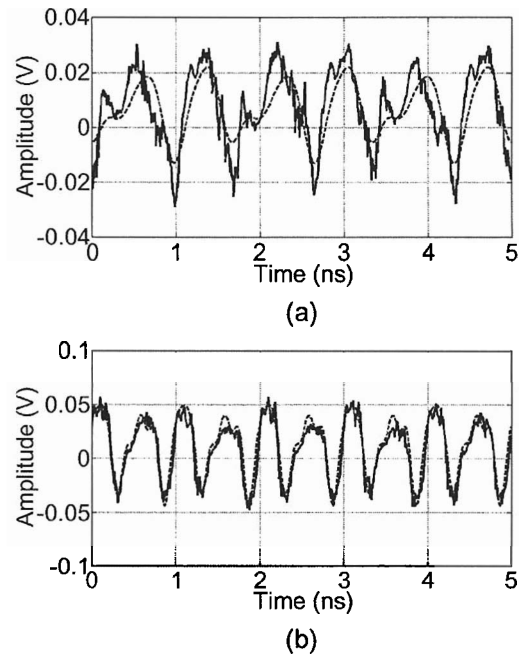

Fig. 11. Measured probe distortion (solid line) and model fit (dashed line) for (a) 600-MHz and (b) 1-GHz data. The signal peak amplitude was 1.6 V.

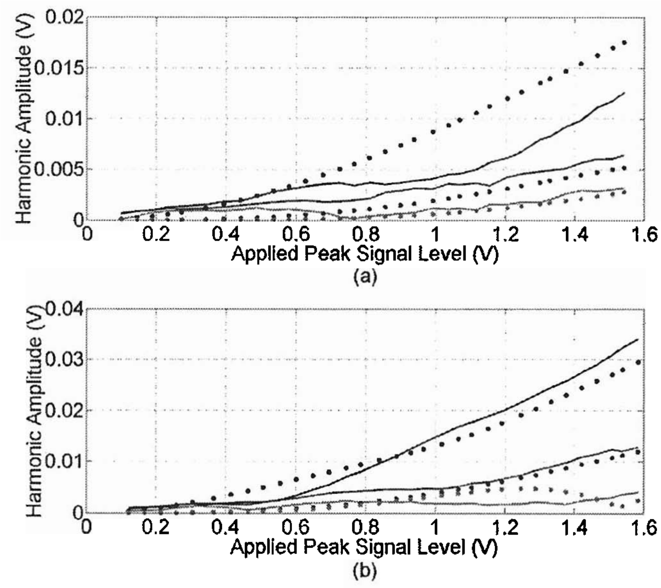

Fig. 12. Measured (solid line) and modeled (dotted line) magnitude of second (darkest), third, and fourth (lightest) harmonics versus input signal level for (a) 600-MHz and (b) 1-GHz measurement ensembles but with $\ddot{y}$ terms excluded from the model.

phase agreement for the third harmonic for signal levels greater than approximately 1 V. Phase agreement for the 600 MHz is not as good, but for signal levels greater than approximately 1.2 V, the phase error for the second and third harmonics is nearly flat. In neither case is the modeled fourth harmonic phase in good agreement with measured data. The reason for this is not clear and warrants further study.

Fig. 11 compares measured probe harmonic distortion with model-generated errors in the time domain. The model fits the 1-GHz data extremely well. The 600-MHz case represents a tradeoff. A higher order model fits the data better but yields inferior distortion performance at frequencies away from the calibration points.

To see the effect of the $\ddot{y}$ terms on the model, the magnitude of the second, third, and fourth harmonics of measured and modeled data are again plotted in Fig. 12 but using a model without the A_2 and A_3 components. In this case, the magnitude response of the model does not agree with measured data as well as it does when the model contains second-derivative terms. In Fig. 13, the effect of excluding the second-derivative

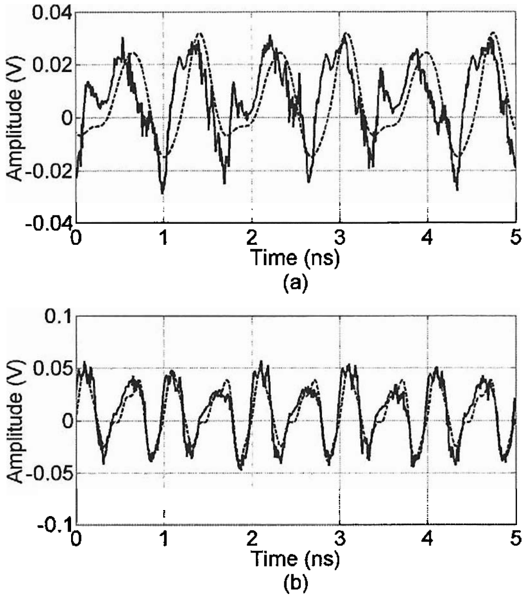

Fig. 13. Measured probe distortion (solid line) and model fit (dashed line) for (a) 600-MHz and (b) 1-GHz data but with $\dddot{y}$ terms excluded from the model. The signal peak amplitude was 1.6 V.

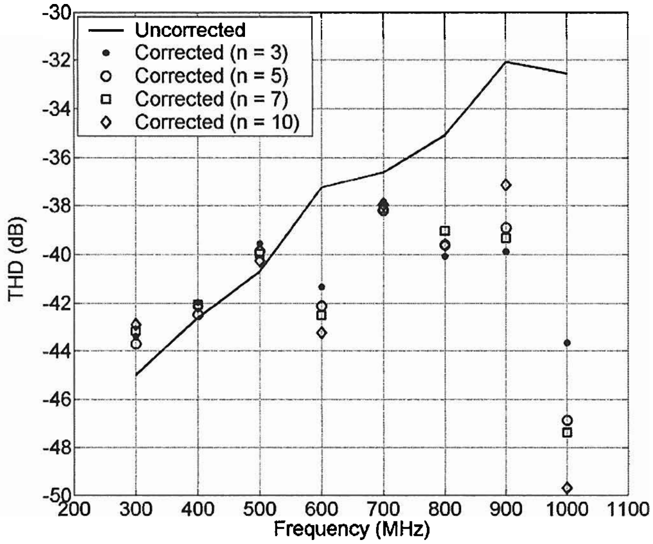

Fig. 14. Probe THD. The peak signal level was 1.6 V.

terms on measured probe distortion is especially evident in the 600-MHz data, where time alignment of the measured and fitted data is not as good as that shown in Fig. 11. Although the structure of the modeled error in Fig. 13(a) differs slightly from that in Fig. 11(a), a more significant effect of the $\boldsymbol{A}_3$ components is to adjust the temporal placement of the $\boldsymbol{A}_1$ components that carry most of the fit. This can be understood in terms of a Taylor series where

$$f(x+\Delta t) \approx f(x) + \Delta t \frac{df(x)}{dt} \tag{7}$$

for small Δ_t and is consistent with the relatively small weights (vectors 11–20 in Fig. 6) associated with the $\boldsymbol{A}_2$ and $\boldsymbol{A}_3$ model vectors. It is noted that the $\boldsymbol{A}_0$ and $\boldsymbol{A}_2$ terms are necessary to achieve the degree of fit shown in Figs. 9–11 even though their coefficients are relatively small.

Fig. 14 shows uncorrected and corrected THD over the frequency range of 300 MHz to 1 GHz. Because the data records for the frequencies other than 600 MHz and 1 GHz did not contain integer numbers of waveform periods, THD was computed by fitting a ten-harmonic model to each data record and computing the ratio of the rms of the ten fitted harmonics to the rms of the fitted fundamental. As might be expected, the degree of improvement correlates with the model order at the frequencies used to calibrate the model, which are -600 MHz and 1 GHz. However, at 900 MHz, the highest order model produces the smallest improvement. The poor performance of the model below 600 MHz is probably explained by the probe-distortion behavior, which departs markedly from the model behavior at these frequencies. The behavior is manifested as comparatively large low-order harmonic components at small signal amplitudes. This behavior is not understood and is the subject of future work. Most significant is that at 800 MHz, 900 MHz, and 1 GHz, model $n = 5$ corrections improve THD by 4, 7, and 14 dB, respectively.

VI. Conclusion

An analytic model for describing the distortion behavior of a high-speed sampling/digitizing probe has been presented. The model, which consists of suitable polynomials in the sampled waveform's instantaneous amplitude and time derivatives, was deduced experimentally from examination of the probe's dynamic error behavior in the phase plane. An ensemble of calibration waveforms was measured with the probe, and the data were then fit via least squares to the model. The polynomial basis functions of the model were found to be good descriptors of the dynamic error behavior of the probe, which was designed for accurate waveform metrology applications. An improvement in harmonic distortion at 1 GHz from -32 to -46 dB was achieved.

References

[1] H. Ku and J. S. Kenney, "Analysis of ACPR performance for memoryless predistorter considering power amplifier memory effects," in *Proc. IEEE Int. Microw. Symp. Dig.*, Jun. 2004, vol. 3, pp. 1863–1866.
[2] K. A. Remley *et al.*, "Phase detrending for measured multisine signals," in *Proc. 61st ARFTG Microw. Meas. Conf. Dig.*, Jun. 13, 2003, pp. 73–83.
[3] D. I. Bergman and B. C. Waltrip, "A low noise latching comparator probe for waveform sampling applications," *IEEE Trans. Instrum. Meas.*, vol. 52, no. 4, pp. 1107–1113, Aug. 2002.
[4] O. B. Laug, T. M. Souders, and D. R. Flach, "A custom integrated circuit comparator for high-performance sampling applications," *IEEE Trans. Instrum. Meas.*, vol. 41, no. 6, pp. 850–855, Dec. 1992.
[5] D. I. Bergman, "Dynamic error correction of a digitizer for time domain metrology," *IEEE Trans. Instrum. Meas.*, vol. 53, no. 5, pp. 1384–1390, Oct. 2004.
[6] *Calibration Services User's Guide*, NIST, Gaithersburg, MD, 1998, pp. 189–193. Special Pub. SP250.
[7] T. A. Rebold and F. H. Irons, "A phase-plane approach to the compensation of high-speed analog-to-digital converters," in *Proc. IEEE Int. Symp. Circ. and Systems*, May 1987, pp. 455–458.
[8] D. Moulin and D. S. Ledwell, "On A/D converter linearization using two-dimensional error-correction tables," in *Proc. Int. Conf. A/D and D/A Conv.*, 1991, pp. 1–6.
[9] H. Wollman and B. N. S. Babu, "Phase plane analysis of high speed A/D converters with sine waves." in *Proc. Int. Conf. A/D and D/A Conv.*. 1991. pp. 40–45.

[10] D. M. Hummels *et al.*, "Characterization of ADCs using a non-iterative procedure," in *Proc. IEEE Int. Symp. Circ. Syst.*, 1994, vol. 2, pp. 5–8.
[11] F. H. Irons *et al.*, "Analog-to-digital converter error diagnosis," in *Proc. IEEE Instrum. Meas. Tech. Conf.*, Jun. 1996, pp. 732–737.
[12] G. M. Kelso *et al.*, "Fast compensation of analog to digital converters," in *Proc. IEEE Instrum. Meas. Tech. Conf.*, 1999, pp. 1295–1298.
[13] D. Moulin, "Real-time equalization of A/D converter nonlinearities," in *Proc. IEEE Int. Symp. Circ. and Systems*, 1989, pp. 262–267.
[14] G. N. Stenbakken and J. P. Deyst, "Time-base nonlinearity determination using iterated sine-fit analysis," *IEEE Trans. Instrum. Meas.*, vol. 47, no. 5, pp. 1056–1061, Oct. 1998.
[15] P. R. Gray and R. G. Meyer, *Analysis and Design of Analog Integrated Circuits*. Hoboken, NJ: Wiley, 1977, p. 56.
[16] *Standard for Terminology and Test Methods for Analog-to-Digital Converters*, IEEE Std. 1241-2000, 2000.
[17] *Standard for Digitizing Waveform Recorders*, IEEE Std. 1057-1994, 1994.
[18] J. P. Deyst and T. M. Souders, "Phase plane compensation of the NIST sampling comparator system," in *Proc. IEEE Instrum. Meas. Tech. Conf.*, 1994.

David I. Bergman (M'99) received the B.S. degree in electrical engineering from the University of Maryland, College Park, in 1988 and the M.S. degree in electrical engineering from the Johns Hopkins University, Baltimore, MD, in 1994.

From 1988 to 1999, he was with the National Aeronautics and Space Administration. Since 1999, he has been with the National Institute of Standards and Technology, Quantum Electrical Metrology Division, Gaithersburg, MD, where he is currently working on the development of precision waveform sampling instrumentation.

Gerard N. Stenbakken (M'71) received the B.S degree in physics from the University of Minnesota in 1963 and the M.S. degree in physics and electrica engineering from the University of Maryland, i 1969 and 1986, respectively.

He is with the National Institute of Standards an Technology, Quantum Electrical Metrology Division, Gaithersburg, MD, where he works on project involving the development of precision electroni instrumentation and testing strategies for comple electronic devices. He helped in the development o the first digital phase angle standard and led the development of an early wideband precision sampling wattmeter. He is currently working on the developmen of next-generation precision electric power instrumentation, test methods, an a calibration system for phase measurement units.